Applied Physics Letters

RESEARCH ARTICLE | OCTOBER 23 2024

Epitaxial $(Al_xGa_{1-x-y}In_y)_2O_3$ alloys lattice matched to monoclinic Ga_2O_3 substrates

Stephen Schaefer ; Michelle Smeaton ; Kingsley Egbo ; Syed Hasan ; William Callahan ; Glenn Teeter ; Andriy Zakutayev ; M. Brooks Tellekamp

Appl. Phys. Lett. 125, 172106 (2024)
https://doi.org/10.1063/5.0238259

Articles You May Be Interested In

Picosecond carrier lifetimes in dilute GaInNAs grown on InP substrate

Appl. Phys. Lett. (October 2011)

Structural characters and band offset of Ga_2O_3–Sc_2O_3 alloys

Appl. Phys. Lett. (February 2022)

Resonant optical in-well pumping of an (AlGaIn)(AsSb)-based vertical-external-cavity surface-emitting laser emitting at 2.35 μ m

Appl. Phys. Lett. (August 2007)

18 November 2024 22:31:25

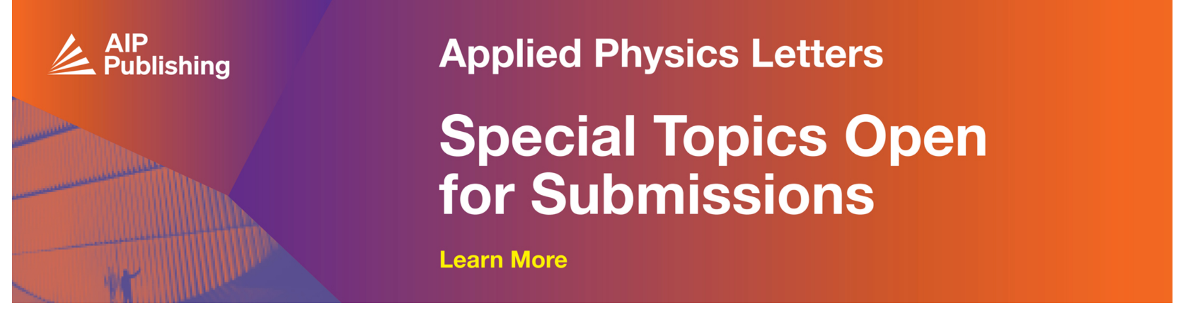

Applied Physics Letters ARTICLE pubs.aip.org/aip/apl

Epitaxial $(Al_xGa_{1-x-y}In_y)_2O_3$ alloys lattice matched to monoclinic Ga_2O_3 substrates

Cite as: Appl. Phys. Lett. **125**, 172106 (2024); doi: 10.1063/5.0238259
Submitted: 10 September 2024 · Accepted: 14 October 2024 ·
Published Online: 23 October 2024

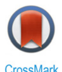

Stephen Schaefer,[a)] Michelle Smeaton, Kingsley Egbo, Syed Hasan, William Callahan, Glenn Teeter, Andriy Zakutayev, and M. Brooks Tellekamp[a)]

AFFILIATIONS

National Renewable Energy Laboratory, Golden, Colorado 80401, USA

[a)]Authors to whom correspondence should be addressed: Stephen.Schaefer@nrel.gov and brooks.tellekamp@nrel.gov

ABSTRACT

We have epitaxially stabilized a series of monoclinic $(Al_xGa_{1-x-y}In_y)_2O_3$ alloys by careful choice of molecular beam epitaxy growth conditions, which balance alloy growth with suboxide desorption. The films are pseudomorphic to (010) β-Ga_2O_3 substrates at thicknesses up to 150 nm with compositions ranging from $(Al_{0.01}Ga_{0.83}In_{0.16})_2O_3$ to $(Al_{0.24}Ga_{0.75}In_{0.03})_2O_3$. The absorption edge shifts from approximately 4.62–5.14 eV with coincidently increasing Al and decreasing In mole fractions. *J–V* measurements reveal an increase in resistivity over four orders of magnitude with a maximum value of 4.2×10^5 Ω-cm for $(Al_{0.17}Ga_{0.76}In_{0.07})_2O_3$, which has nearly identical lattice parameters (both in-plane and out-of-plane) to the underlying β-Ga_2O_3. Scanning transmission electron microscopy of this sample reveals a mostly uniform and single crystalline film, though we identify areas of non-uniform In incorporation and some γ-phase inclusions. This work demonstrates the feasibility of thick layers lattice-matched to β-Ga_2O_3 with increased bandgap compared to phase-separation limited $(Al,Ga)_2O_3$. These alloys can enable higher bandgap epitaxial dielectrics and high sheet charge density transistors by increasing the conduction band offset with respect to β-Ga_2O_3.

© 2024 Author(s). All article content, except where otherwise noted, is licensed under a Creative Commons Attribution (CC BY) license (https://creativecommons.org/licenses/by/4.0/). https://doi.org/10.1063/5.0238259

18 November 2024 22:31:25

Gallium oxide (Ga_2O_3) is an ultra-wide bandgap semiconductor with potential to displace existing materials such as SiC and GaN for high power and/or extreme operating environment devices. The stable monoclinic β-phase with symmetry *C2/m* has a direct bandgap energy of 4.76 eV (Ref. 1) and theoretical critical field as high as 8 MV/cm (Refs. 2 and 3) and exhibits controllable n-type doping by Sn, Ge, and Si[4–7] in addition to large area wafer growth from melt.[3,4,6,8] Isovalent alloying of In and Al in β-Ga_2O_3 tunes the bandgap energy and epilayer strain, with theoretically achievable bandgap energies in the range of 7.2–7.5 eV for monoclinic θ-Al_2O_3 (Refs. 9 and 10) to 2.7 eV for monoclinic In_2O_3.[11,12]

Band engineering in the $(Al_xGa_{1-x})_2O_3$ alloy system is challenging due to the limitations of strain relaxation, with pseudomorphic layers typically limited to 20% Al mole fraction or less[13] to avoid poor crystal quality and separation into competing phases. This limits the achievable sheet charge density and therefore channel conductivity of transistors,[5,14] which rely on the large conduction band offset between a wider bandgap layer (i.e., Al-rich alloy) and a smaller bandgap layer (i.e., Ga_2O_3 or In-rich alloy). Solutions to increase the conduction band offset in the transistor barrier layer, without loss of crystalline phase or structural quality, could significantly improve the performance of Ga_2O_3 transistors. Likewise, epitaxial dielectric layers with large conduction band offset and low interface and bulk defect density are needed for gallium oxide MOS devices.[15] Additionally, bandgap tunability enables Ga_2O_3-based UV photodetectors[16,17] with absorption onset spanning the entire UVC spectrum (200–280 nm).

Epitaxial growth of ternary monoclinic $(Al_xGa_{1-x})_2O_3$ and $(In_yGa_{1-y})_2O_3$ alloys has been demonstrated by a variety of techniques including MBE,[18,19] MOCVD,[20,21] and PLD.[22,23] We recently investigated the $(In_yGa_{1-y})_2O_3$ growth space and identified growth conditions that allow indium incorporation through cyclical growth and etching.[18] Incorporating both Al and In in the quaternary alloy $(Al_xGa_{1-x-y}In_y)_2O_3$ could provide an additional degree of freedom, permitting independent control of both bandgap energy and epilayer strain. This would enable growth of nearly lattice matched layers on β-Ga_2O_3, which are not limited by strain relaxation or phase separation. Lattice matched quaternary alloys with increased bandgap energy have been realized in the (AlGaIn)N/GaN[24] and (AlGaIn)As/InP[25] systems but have yet to be demonstrated in oxides due to the growth challenges associated with suboxide kinetics, which make indium

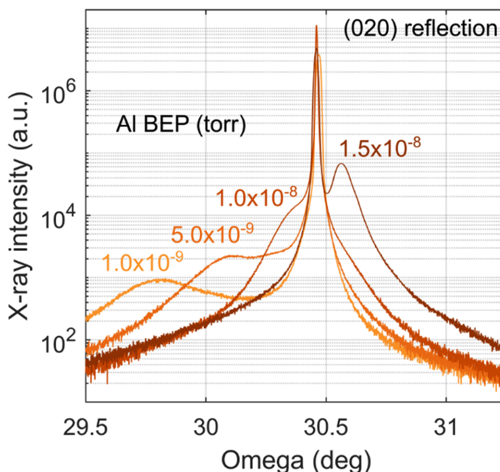

FIG. 1. Coupled ω-2θ XRD scans of the (020) plane for $(Al_xGa_{1-x-y}In_y)_2O_3$ films grown on (010) oriented β-Ga_2O_3 substrates.

incorporation difficult at standard growth conditions.[18,19] As a result, there are no experimental demonstrations of monoclinic $(Al_xGa_{1-x-y}In_y)_2O_3$ alloys; however, first-principles calculations of the electronic properties have been reported.[11]

In this work, we report synthesis of monoclinic $(Al_xGa_{1-x-y}In_y)_2O_3$ epilayers pseudomorphic to Ga_2O_3 substrate. The structural, chemical, optical, and electrical properties of the films are investigated by x-ray diffraction (XRD), x-ray photoelectron spectroscopy (XPS), atomic force microscopy (AFM), spectroscopic ellipsometry (SE), *J–V* measurements, scanning transmission electron microscopy (STEM), and energy-dispersive x-ray spectroscopy (EDS). An absorption edge energy of 5.14 eV and resistivity of 4.2×10^5 Ω-cm are achieved for $(Al_{0.17}Ga_{0.76}In_{0.07})_2O_3$ with nearly identical lattice constants as the underlying β-Ga_2O_3 substrate. These results should lead to increased conduction band offset with respect to β-Ga_2O_3 and enable higher bandgap epitaxial dielectrics for high sheet charge density transistors.

Four β-$(Al_xGa_{1-x-y}In_y)_2O_3$ films were grown on (010) oriented Fe doped $10 \times 10\,mm^2$ β-Ga_2O_3 wafers (Novel Crystal Technology). The details on wafer cleaning, the MBE system, source materials, calibration, and growth temperature calibration are described in Ref. 18. The growth temperature was 750 °C for all samples. Ga and In beam equivalent pressures (BEP) were fixed at 5.0×10^{-8} and 2.0×10^{-7} Torr, respectively, while Al BEP varied from 1.0×10^{-9} to 1.5×10^{-8} Torr. Taking into account the varying oxidation efficiencies and sensitivity factors[18,26] for Ga, Al, and In, the growths are all oxygen-rich with flux ratio (3/2)(III/O) ranging from 0.45 to 0.67. Further details on flux calculations are provided in the supplementary material.

Figure 1 shows symmetric XRD scans of the (020) plane for the four samples, illustrating a clear shift in the out-of-plane lattice constant, consistent with epilayer strain to the β-Ga_2O_3 substrate shifting from compressive (In-rich) to tensile (Al-rich) as the Al flux increases. All other growth conditions, including In flux, are held constant. XPS depth profiling reveals approximately uniform composition in the growth direction with some variation close to the interface (supplementary material Fig. 7). The thickness-averaged cation compositions are reported in Table I, with Al mole fractions in the range of 1.4%–24.4% and In mole fractions in the range of 3.1%–15.5%. The Al mole fraction increases linearly with Al flux, indicating a unity sticking coefficient consistent with previous reports.[13,27] By reducing the Ga flux and growing under oxygen-rich conditions at 750 °C, significant In incorporation is achieved.[18] In non-equilibrium MBE growth, energetic barriers to Al and Ga adatom migration at typical MBE growth conditions result in "frozen-in" surface reconstructions[28] with net tensile strain. Incorporation of In adatoms is expected to lower the total surface energy by reducing the tensile strain, and the addition of comparatively low Al flux (1×10^{-9} Torr BEP) results in greatly enhanced In incorporation (15% In mole fraction) compared to $(In_yGa_{1-y})_2O_3$ grown under similar conditions without Al (~5% In mole fraction).[18]

To analyze strain and composition, reciprocal space maps (RSMs) of the (420) and (022) planes were measured. Figure 2 shows RSMs of the (420) plane for each sample, and along with the (022) RSMs given in the supplementary material, pseudomorphic growth along both a- and c-axes is confirmed. The films grown with Al BEP $= 5 \times 10^{-9}$–1.5×10^{-8} are pseudomorphic and coherently

TABLE I. Cation atomic concentrations (cation mole fractions) in $(Al_xGa_{1-x-y}In_y)_2O_3$. Methods include (i) thickness-averaged XPS depth profiles and (ii) self-consistent solution of Vegard's law and strained lattice constants identified in (420) and (022) RSMs with Al concentration fixed to XPS value. Long-range crystal quality is demonstrated by rocking curve FWHM values from on-axis (020) and off-axis (420) reflections—broad and narrow indicate where two peaks were used to fit the rocking curve. The lattice constants for β-Ga_2O_3 are listed for comparison.[29]

		Atomic concentration (mole fraction) (%)			Lattice constant (Å)			Rocking curve FWHM (arc sec)	
Al BEP (Torr)	Method	Al	Ga	In	*a*	*b*	*c*	(020)	(420)
1×10^{-9}	XPS	0.6 (1.4)	33.2 (83.1)	6.3 (15.5)	12.261	3.090	5.861	Broad: 3390	3100
	RSM		34.3 (85.8)	5.1 (12.8)				Narrow: 253	
5×10^{-9}	XPS	3.4 (8.5)	32.7 (81.7)	4.0 (9.8)	12.245	3.058	5.823	Broad: 2180	1990
	RSM		33.2 (82.9)	3.4 (8.6)				Narrow: 207	
1.0×10^{-8}	XPS	6.8 (16.8)	30.6 (76.5)	2.7 (6.7)	12.214	3.037	5.798	...	1300
	RSM		30.9 (77.3)	2.4 (5.9)				174	
1.5×10^{-8}	XPS	9.7 (24.4)	29.0 (72.5)	1.2 (3.1)	12.220	3.024	5.810	...	352
	RSM		27.7 (69.2)	2.6 (6.4)				122	
...	Ref. 29			β-Ga_2O_3	12.214	3.0371	5.7981		

18 November 2024 22:31:25

© Author(s) 2024

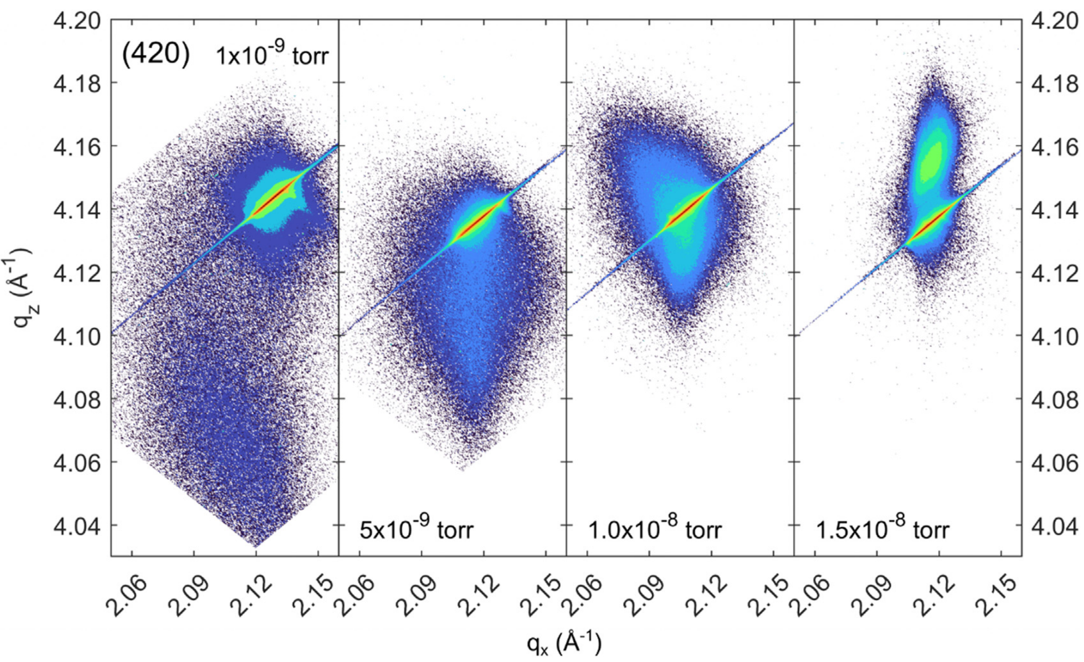

FIG. 2. (420) plane reciprocal space maps of $(Al_xGa_{1-x-y}In_y)_2O_3$ alloys grown at 750 °C, Ga BEP = 5.0×10^{-8} Torr, and In BEP = 2.0×10^{-7} Torr. Al BEP is labeled for each map.

strained to the β-Ga_2O_3 substrate, while the most compressively strained film grown with Al BEP = 1×10^{-9} is partially relaxed. Pendellösung fringes in the (022) RSM indicate good structural quality and a thickness of 130 nm for the most Al-rich (In-poor) film. Long-range crystal quality was investigated by symmetric and asymmetric rocking curves (Table I) showing a reduction in FWHM for increasing (decreasing) aluminum (indium). Coincidentally, the films with a higher crystalline quality show a decreased RMS roughness as measured by AFM. The strained lattice constants are directly identified from the RSMs using a custom Python 2D peak finding routine and reported in Table I. Notably, the film grown with Al BEP = 1.0×10^{-8} Torr has nominally identical lattice parameters to β-Ga_2O_3 despite large Al and In compositions.

Assuming Al mole fraction given by the XPS measurements in Table I, the In mole fraction can be calculated from these lattice constants by self-consistently solving Vegard's law and the elastic strain equations as described in the supplementary material. The resulting In mole fractions match those measured by XPS to within 3% mole fraction across the entire composition range, confirming the validity of Vegard's law interpolation of binary monoclinic Al_2O_3 and In_2O_3 lattice constants. Table I reports these compositions, showing good agreement for the In mole fraction for both methods.

Figure 3(a) shows the absorption onset measured by SE for the four $(Al_xGa_{1-x-y}In_y)_2O_3$ samples and reference (010) oriented Fe-doped β-Ga_2O_3. The Tauc plot shows the quantity $(\alpha \cdot h\nu)^{1/\gamma}$, which is proportional to the absorption coefficient α assuming direct dipole-allowed optical transitions with power law $\gamma = 1/2$ dependence on photon energy $h\nu$. The most In-rich (Al-poor) sample exhibits significant sub-bandgap absorption below 4.3 eV. The sub-gap absorption may be the result of a variety of factors including localized strain, clustering of In atoms, or γ-phase $(InGa)_2O_3$ or bixbyite In_2O_3 phase inclusions.[30] The other $(Al_xGa_{1-x})_2O_3$ samples exhibit a sharp absorption edge that increases in photon energy with increasing (decreasing) Al (In) content. Fits to the linear portion of the Tauc plot absorption spectra determine the direct dipole-allowed optical gap energy of the $(Al_xGa_{1-x-y}In_y)_2O_3$ samples. Here, we distinguish between the bandgap energy, which is the lowest transition energy between the valence and conduction bands in a perfectly ordered crystal, and the optical gap energy measured by SE, which is influenced by a variety of factors including strain,[9] defects,[31] cation site disorder and/or clustering, free carriers,[32] and phase inclusions.[30] The polarization of light in the SE measurements of the (010) oriented films contains components parallel to the z axis[33] and therefore is sensitive to direct transitions at the Γ point approximately 30 meV higher than the fundamental indirect transition in β-Ga_2O_3 (see the supplementary material for further discussion).[32–34]

Figure 3(b) shows the optical gap energy vs pseudocubic lattice constant, calculated as the cube root of the strained unit cell volume obtained from the RSMs. First-principles calculations[11] of the direct bandgap energy of relaxed $(AlGaIn)_2O_3$ interpolated to the experimental compositions are shown by open squares. Bandgap bowing curves are shown by dashed black lines with lattice-matched $(Al_xGa_{1-x-y}In_y)_2O_3$ shown by the dotted gray line. The monoclinic Al_2O_3 and In_2O_3 bandgap energies are 7.34 (Ref. 9) and 2.78 eV,[12] respectively, with lattice parameters listed in the supplementary material. The $(AlGa)_2O_3$ and $(InGa)_2O_3$ bandgap bowing parameters are 0.64 (Ref. 9) and 0.36 eV,[30] respectively. The nearly lattice-matched $(Al_{0.17}Ga_{0.76}In_{0.07})_2O_3$ sample grown with Al BEP = 1.0×10^{-8} Torr exhibits an optical gap of 5.07 eV and an increase of 0.13 eV with respect to Ga_2O_3. The measured optical gap is in good agreement with

18 November 2024 22:31:25

© Author(s) 2024

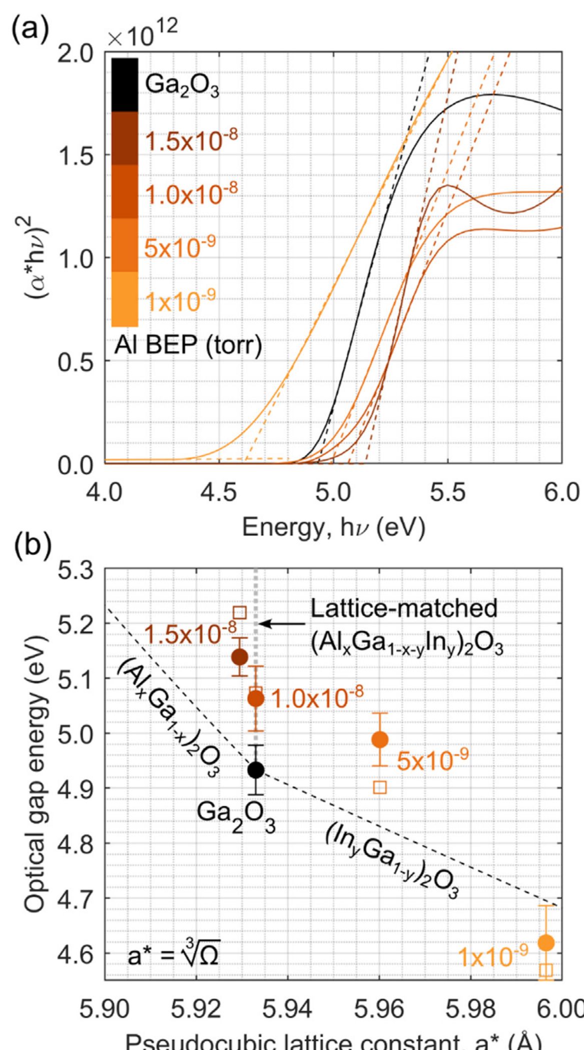

FIG. 3. Absorption onset for $(Al_xGa_{1-x-y}In_y)_2O_3$ alloys. (a) Tauc plot of $(\alpha \cdot h\nu)^2$ vs photon energy $h\nu$. Fits to linear portion of spectra are shown by dashed lines. Reference (010) β-Ga_2O_3 shown by black curve. (b) Optical gap energy (filled circles) extrapolated from Tauc plot fits vs strained pseudocubic lattice constant, with fit error shown by bars. First-principles calculations[11] of direct bandgap energy of relaxed $(AlGaIn)_2O_3$ shown by open squares. Bandgap bowing for $(Al_xGa_{1-x})_2O_3$ and $(In_yGa_{1-y})_2O_3$ shown by dashed black lines. Al BEP in Torr labeled for each sample.

first-principles calculations showing a direct bandgap energy of 5.08 eV for a relaxed alloy of the same composition.[11] Assuming a type-II staggered band offset with 89% of band offset due to the conduction band discontinuity as in $(Al_xGa_{1-x})_2O_3$,[35] the conduction band offset of this lattice-matched sample is approximately 0.12 eV, or $4.5\times k_BT$ at room temperature. First-principles calculations predict a conduction band offset of 0.45 eV for $(Al_{0.2}Ga_{0.8})_2O_3$ with respect to Ga_2O_3.[35] Larger Al mole fractions in $(AlGaIn)_2O_3$ are required to match or exceed the conduction band offset in $(AlGa)_2O_3$; however, the absence of strain relaxation or competing crystal phases in lattice-matched $(AlGaIn)_2O_3$ recommend the quaternary alloy for high structural quality heterojunctions in HEMTs or gate dielectrics in FETs.

Annular electrical test structures were fabricated on the sample surfaces with an inner Ni/Au anode and outer Ti/Au cathode separated by a 10 μm gap. Figure 4(a) shows the current–voltage characteristics of the structures with 300 μm diameter Ni/Au anode. Figure 4(b) shows the bulk resistivity as a function of Al flux for five different anode diameters in the range of 50–300 μm. The device resistance is calculated from the differential resistance at +10 V bias, and the bulk resistivity is determined from the sheet resistance, which can be related

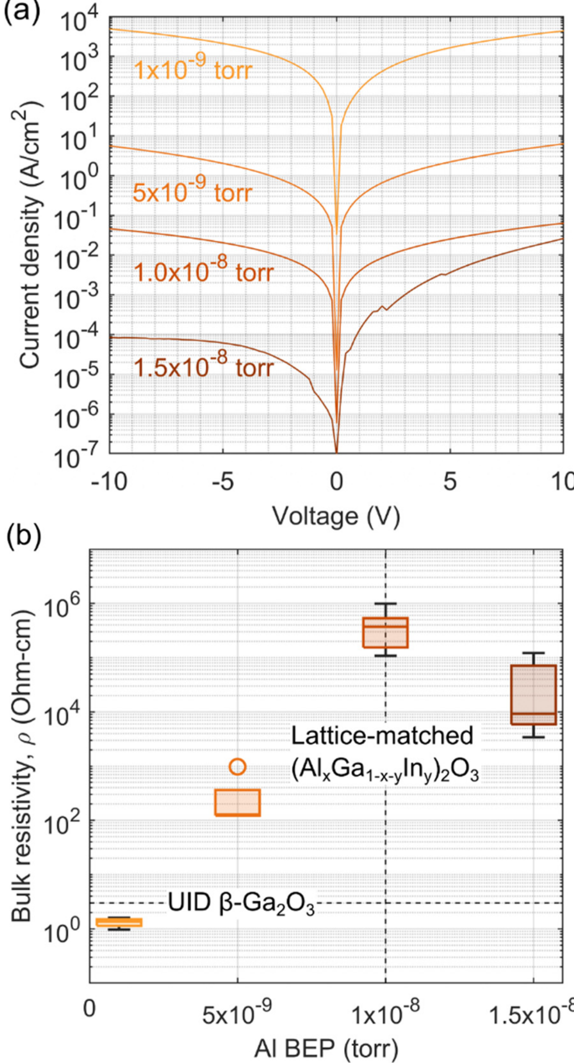

FIG. 4. Electrical characteristics of annular test structures. (a) Current–voltage characteristics of 300 μm pad diameter devices and (b) bulk resistivity ρ as a function of Al flux evaluated at +10 V bias for all pad diameters. Boxes and whiskers indicate interquartile and maximum/minimum ranges, respectively. Circular markers indicate outliers greater than 1.5× the interquartile range. Typical resistivity of MBE-grown β-Ga_2O_3 shown by dashed horizontal line.[15]

18 November 2024 22:31:25

© Author(s) 2024

to specific resistivity by a geometric factor assuming negligibly small transfer length. This is a valid assumption when the epilayer sheet resistance is much greater than the contact sheet resistance (details in the supplementary material).[36]

The most Al-rich sample exhibits weakly rectifying behavior, while the other three samples display high reverse leakage current and approximately Ohmic behavior. The mean resistivity increases with increasing (decreasing) Al (In) content from 1.3 Ω-cm to a maximum of 4.2×10^5 Ω-cm for the lattice-matched $(Al_{0.17}Ga_{0.76}In_{0.07})_2O_3$ sample. Despite its larger bandgap energy, the Al-rich $(Al_{0.24}Ga_{0.73}In_{0.03})_2O_3$ sample is less resistive than the lattice-matched sample, possibly due to an increased defect density caused by lattice mismatch to the Ga_2O_3 substrate. The resistivity of the $(Al_{0.17}Ga_{0.76}In_{0.07})_2O_3$ sample is significantly larger than the $\sim$3 Ω-cm resistivity typical of unintentionally doped β-Ga_2O_3 grown by MBE.[15] Additional processing and characterization including Hall effect, transfer length measurements, and temperature-dependent *J–V* are needed to fully understand the electrical properties of the $(AlGaIn)_2O_3$ layers.

STEM imaging of the nearly lattice-matched $(Al_{0.17}Ga_{0.76}In_{0.07})_2O_3$ sample grown with Al BEP = 1.0×10^{-8} Torr reveals the alloy's microstructure. Figure 5(a) shows a high angle annular dark field (HAADF) STEM image of the growth interface, confirming pseudomorphic growth of monoclinic $(AlGaIn)_2O_3$. Facets along the [110] direction with an approximate angle of 14° with respect to the interface are due to the preparatory Ga etch step prior to film growth and have been reported on (010) oriented β-Ga_2O_3 surfaces.[37] The faceting gives rise to a diagonal contrast motif that is particularly pronounced in the HAADF STEM image in Fig. 5(b). This motif is less pronounced in medium-angle annular dark-field (MAADF) images (not shown), indicating that the contrast is due to compositional variation rather than local strain. As $(AlGaIn)_2O_3$ growth progresses in the [010] direction, bright columnar contrast regions develop, suggesting lateral composition non-uniformity. This is evident in EDS maps of Ga, Al, and In in Figs. 5(c)–5(e), which show approximately uniform Al incorporation and enhanced In incorporation in the bright columnar regions that is anticorrelated to Ga. In incorporation is locally enhanced in the troughs of the [110] oriented facets near the wafer/epilayer interface; however, the origin of the extended columnar regions does not show a clear relation to the facets. Uniform Al incorporation is consistent with reported MBE growth of $(Al_xGa_{1-x})_2O_3$ where all Al flux incorporates,[13,27] while the non-uniform In distribution points to the possible role that localized strain[38] and kinetically inhibited adatom mobility due to the high oxidation efficiency of In[39] may play in its incorporation.

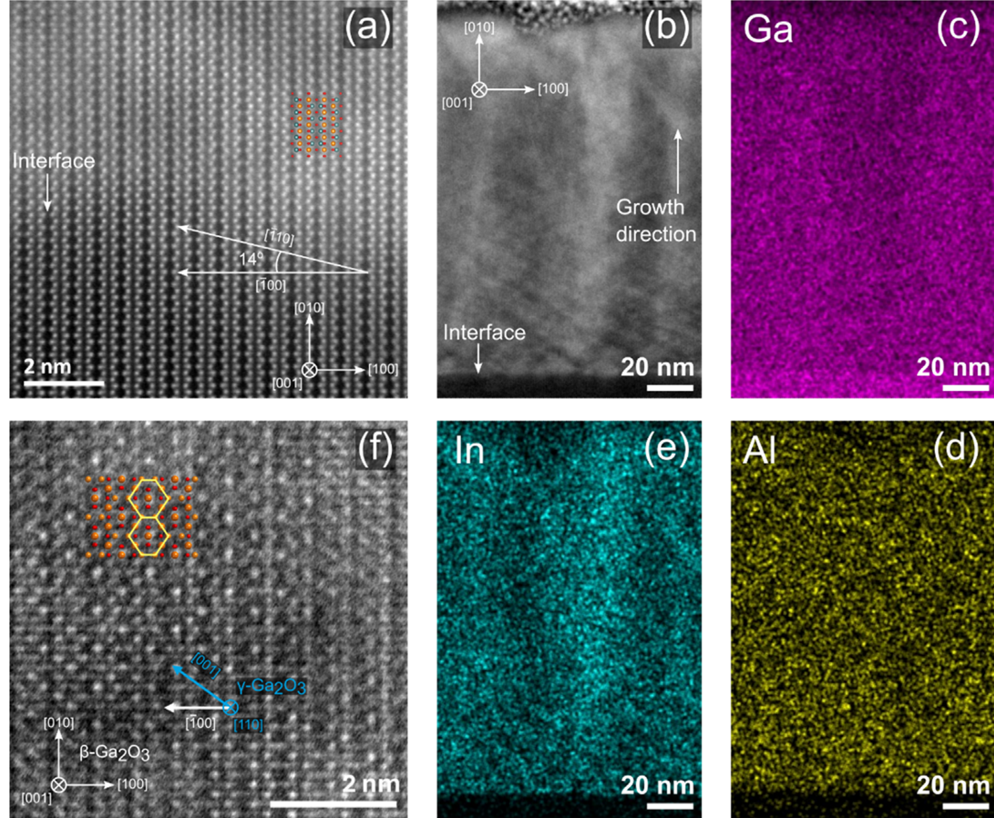

FIG. 5. STEM images and EDS maps along [001] zone axis of nearly lattice-matched 158 nm thick $(AlGaIn)_2O_3$ with Al BEP = 1.0×10^{-8} Torr. (a) HAADF-STEM image showing interface between β-Ga_2O_3 wafer and $(AlGaIn)_2O_3$ epilayer. Atomic model of β-Ga_2O_3 overlaid. [110] oriented facet due to Ga etch at the wafer–epilayer interface shown by white lines. (b) HAADF-STEM image highlighting diagonal mass-contrast motif near interface. (c)–(e) EDS maps of cation composition for the field of view shown in (b). (f) [110] oriented γ-Ga_2O_3 phase inclusion. Atomic model shown with γ-Ga_2O_3 hexagonal motifs highlighted in yellow.

18 November 2024 22:31:25

© Author(s) 2024

Inclusions of γ-$(AlGaIn)_2O_3$ (space group Fd $\bar{3}$ m) is observed sporadically throughout the film. Figure 5(f) shows one such phase inclusion with an atomic model overlaid. The γ-phase [110] direction is parallel to the β-Ga_2O_3 [001] zone axis, with angle of approximately 36° between the γ-phase [001] direction and β-phase [010] growth direction. Similar γ-phase inclusions were reported in Ref. 34 with identical orientation. γ-phase inclusions have been reported in the growth of the ternary alloy $(Al_xGa_{1-x})_2O_3$ by methods including MBE[28,40] and MOCVD.[28] The observed γ-phase inclusions are irregularly shaped and do not show a clear relationship with compositional inhomogeneity or extended defects, making identification of a phase transformation mechanism difficult. Chang *et al.*[40] suggested a high concentration of Ga interstitials may be responsible for γ-phase formation on the β-Ga_2O_3 (010) surface. In contrast, Johnson *et al.*[28] found planar defects that resemble the γ-phase and consist of split vacancies and displaced octahedrally coordinated (Al,Ga) atoms. Al incorporation is increased in the vicinity of these planar defects.[28] The picture is complicated by the addition of In. Significant energy barriers to adatom migration occur in non-equilibrium MBE growth,[28] and therefore in the absence of extended defects, we may speculate that local surface reconstruction changes drive the formation of the γ-phase in $(AlGaIn)_2O_3$ where the local strain environment can vary greatly.

This work presents growth of pseudomorphic monoclinic $(Al_xGa_{1-x-y}In_y)_2O_3$ on β-Ga_2O_3. MBE growth at 750 °C, oxygen rich growth, and Ga-limited fluxes are critical for both Al and In incorporation in the monoclinic structure. The Al and In mole fractions are in the range of 1.4%–24.4% and 3.1%–15.5%, respectively. Reciprocal space maps confirm pseudomorphic growth, and lattice-match to β-Ga_2O_3 is achieved for $(Al_{0.17}Ga_{0.76}In_{0.07})_2O_3$ where we observe a-, b-, and c-parameters nearly identical to β-Ga_2O_3. A sharp optical absorption edge is observed for the three samples with highest Al content, and the optical gap energy increases monotonically with increasing Al mole fraction in the range of 4.62–5.14 eV. Lateral electrical devices exhibit approximately Ohmic behavior with an increase in bulk resistivity at forward bias by five orders of magnitude up to 4.2×10^5 Ω-cm for lattice-matched $(Al_{0.17}Ga_{0.76}In_{0.07})_2O_3$. STEM images of this lattice-matched sample indicate uniform Al incorporation but inhomogeneous In incorporation, which is presented as a diagonal motif along [110] facets and progresses to columnar regions along the [010] growth direction. Scattered γ-$(AlGaIn)_2O_3$ phase inclusions are observed, but their volume density is insufficient to significantly affect the bulk properties measured by XRD and SE. The work establishes an MBE growth window for future synthesis of thick monoclinic $(Al_xGa_{1-x-y}In_y)_2O_3$ layers and their possible applications in HEMTs, MOS devices, and UV photodetectors.

See the supplementary material for the details of characterization methods, MBE flux calculations, determination of $(Al_xGa_{1-x-y}In_y)_2O_3$ composition from RSMs and XPS, optical constants and Tauc plot fits, and current–voltage characteristics available online.

This work was authored by the National Renewable Energy Laboratory (NREL), operated by Alliance for Sustainable Energy, LLC, for the U.S. Department of Energy (DOE) under Contract No. DE-AC36-08GO28308. Funding provided by the Laboratory Directed Research and Development (LDRD) Program at NREL (epitaxial growth and structural characterization), and by the Office of Energy Efficiency and Renewable Energy (EERE), Advanced Materials & Manufacturing Technologies Office (AMMTO, electrical and microscopy measurements). The views expressed in the article do not necessarily represent the views of the DOE or the U.S. Government.

AUTHOR DECLARATIONS

Conflict of Interest

The authors have no conflicts to disclose.

Author Contributions

Stephen Schaefer: Conceptualization (equal); Data curation (lead); Formal analysis (lead); Investigation (lead); Methodology (lead); Software (lead); Visualization (lead); Writing – original draft (lead); Writing – review & editing (equal). **Michelle Smeaton:** Data curation (supporting); Formal analysis (supporting); Investigation (equal); Visualization (equal); Writing – review & editing (equal). **Kingsley Egbo:** Investigation (equal); Methodology (equal); Visualization (supporting); Writing – review & editing (supporting). **Syed Hasan:** Formal analysis (supporting); Investigation (equal); Methodology (equal). **Will Callahan:** Data curation (equal); Formal analysis (equal); Methodology (equal); Visualization (equal); Writing – review & editing (supporting). **Glenn Teeter:** Formal analysis (supporting); Investigation (equal); Methodology (equal); Writing – review & editing (supporting). **Andriy Zakutayev:** Conceptualization (equal); Funding acquisition (equal); Supervision (equal); Writing – review & editing (equal). **M. Brooks Tellekamp:** Conceptualization (lead); Formal analysis (equal); Funding acquisition (equal); Investigation (equal); Methodology (equal); Project administration (lead); Resources (equal); Supervision (lead); Validation (equal); Writing – review & editing (equal).

DATA AVAILABILITY

The data that support the findings of this study are available within the article and its supplementary material.

REFERENCES

[1] T. Matsumoto, M. Aoki, A. Kinoshita, and T. Aono, "Absorption and reflection of vapor grown single crystal platelets of β-Ga_2O_3," Jpn. J. Appl. Phys. Part 1 **13**, 1578 (1974).

[2] M. Higashiwaki, K. Sasaki, A. Kuramata, T. Masui, and S. Yamakoshi, "Gallium oxide (Ga_2O_3) metal-semiconductor field-effect transistors on single-crystal β-Ga_2O_3 (010) substrates," Appl. Phys. Lett. **100**, 013504 (2012).

[3] A. Kuramata, K. Koshi, S. Watanabe, Y. Yamaoka, T. Masui, and S. Yamakoshi, "High-quality β-Ga_2O_3 single crystals grown by edge-defined film-fed growth," J. Appl. Phys. **55**, 1202A2 (2016).

[4] M. Higashiwaki, K. Sasaki, H. Murakami, Y. Kumagai, A. Koukitu, A. Kuramata, T. Masui, and S. Yamakoshi, "Recent progress in Ga_2O_3 power devices," Semicond. Sci. Technol. **31**, 034001 (2016).

[5] E. Ahmadi, O. S. Koksaldi, X. Zheng, T. Mates, Y. Oshima, U. K. Mishra, and J. S. Speck, "Demonstration of β-$(Al_xGa_{1-x})_2O_3$/β-Ga_2O_3 modulation doped field-effect transistors with Ge as dopant grown via plasma-assisted molecular beam epitaxy," Appl. Phys. Express **10**, 071101 (2017).

[6] S. J. Pearton, J. Yang, P. H. Cary IV, F. Ren, J. Kim, M. J. Tadjer, and M. A. Mastro, "A review of Ga_2O_3 materials, processing, and devices," Appl. Phys. Rev. **5**, 011301 (2018).

[7] Y. Zhang and J. S. Speck, "Importance of shallow hydrogenic dopants and material purity of ultra-wide bandgap semiconductors for vertical power electron devices," Semicond. Sci. Technol. **35**, 125018 (2020).

18 November 2024 22:31:25

© Author(s) 2024

[8]K. N. Heinselman, D. Haven, A. Zakutayev, and S. B. Reese, "Projected cost of gallium oxide wafers from edge-defined film-fed crystal growth," Cryst. Growth Des. **22**(8), 4854–4863 (2022).
[9]R. Korlacki, M. Hilfiker, J. Knudtson, M. Stokey, U. Kilic, A. Mauze, Y. Zhang, J. Speck, V. Darakchieva, and M. Schubert, "Strain and composition dependencies of the near-band-gap optical transitions in monoclinic $(Al_xGa_{1-x})_2O_3$ alloys with coherent biaxial in-plane strain on Ga_2O_3 (010)," Phys. Rev. Appl. **18**, 064019 (2022).
[10]H. Peelaers, J. B. Varley, J. S. Speck, and C. G. Van de Walle, "Structural and electronic properties of Ga_2O_3-Al_2O_3 alloys," Appl. Phys. Lett. **112**, 242101 (2018).
[11]X. Liu and C.-K. Tan, "Electronic properties of monoclinic $(In_xGa_{1-x})_2O_3$ alloys by first-principle," AIP Adv. **9**, 035318 (2019).
[12]H. Peelaers, D. Steiauf, J. B. Varley, A. Janotti, and C. G. Van de Walle, "$(In_xGa_{1-x})_2O_3$ alloys for transparent electronics," Phys. Rev. B **92**, 085206 (2015).
[13]S. W. Kaun, F. Wu, and J. S. Speck, "β-$(Al_xGa_{1-x})_2O_3/Ga_2O_3$ (010) heterostructures grown on β-Ga_2O_3 (010) substrates by plasma-assisted molecular beam epitaxy," J. Vac. Sci. Technol. A **33**(4), 041508 (2015).
[14]R. Singh, T. R. Lenka, D. K. Panda, R. T. Velpula, B. Jain, H. Q. T. Bui, and H. P. T. Nguyen, "The dawn of Ga_2O_3 HEMTs for high power electronics - A review," Mater. Sci. Semicond. Process. **119**, 105216 (2020).
[15]A. J. Green, J. Speck, G. Xing *et al.*, "β-Gallium oxide power electronics," APL Mater. **10**, 029201 (2022).
[16]H.-Y. Lee, J.-T. Liu, and C.-T. Lee, "Modulated Al_2O_3-Alloyed Ga_2O_3 materials and deep ultraviolet photodetectors," IEEE Photonics Technol. Lett. **30**, 6 (2018).
[17]Z. Zhang, H. von Wenckstern, J. Lenzner, M. Lorenz, and M. Grundmann, "Visible-blind and solar-blind ultraviolet photodiodes based on $(In_xGa_{1-x})_2O_3$," Appl. Phys. Lett. **108**, 123503 (2016).
[18]S. Schaefer, D. Febba, K. Egbo, G. Teeter, A. Zakutayev, and B. Tellekamp, "Rapid screening of molecular beam epitaxy conditions for monoclinic $(In_xGa_{1-x})_2O_3$ alloys," J. Mater. Chem. A **12**, 5508–5519 (2024).
[19]P. Vogt, A. Mauze, F. Wu, B. Bonef, and J. S. Speck, "Metal-oxide catalyzed epitaxy (MOCATAXY): the example of the O plasma-assisted molecular beam epitaxy of β-$(Al_xGa_{1-x})_2O_3/\beta$-$Ga_2O_3$ heterostructures," Appl. Phys. Express **11**, 115503 (2018).
[20]P. Ranga, A. Rishinaramangalam, J. Varley, A. Bhattacharyya, D. Feezell, and S. Krishnamoorthy, "Si-doped β-$(Al_{0.26}Ga_{0.74})_2O_3$ thin films and heterostructures grown by metalorganic vapor-phase epitaxy," Appl. Phys. Express **12**, 111004 (2019).
[21]M. Baldini, D. Gogova, K. Irmscher, M. Schmidbauer, G. Wagner, and R. Fornari, "Heteroepitaxy of $Ga_{2(1-x)}In_{2x}O_3$layers by MOVPE with two different oxygen sources," Cryst. Res. Technol. **49**(8), 552–557 (2014).
[22]R. Wakabayashi, K. Yoshimatsu, M. Hattori, J.-S. Lee, O. Sakata, and A. Ohtomo, "Epitaxial stabilization of complete solid-solution β-$(Al_xGa_{1-x})_2O_3$ (100) films by pulsed-laser deposition," Cryst. Growth Des. **21**(5), 2844–2849 (2021).
[23]H. von Wenckstern, D. Splith, M. Purfürst, Z. Zhang, C. Kranert, S. Müller, M. Lorenz, and M. Grundmann, "Structural and optical properties of $(In,Ga)_2O_3$ thin films and characteristics of Schottky contacts thereon," Semicond. Sci. Technol. **30**, 024005 (2015).
[24]T. Lim, R. Aidam, L. Kirste, P. Waltereit, R. Quay, S. Müller, and O. Ambacher, "Compositional variation of nearly lattice-matched InAlGaN alloys for high electron mobility transistors," Appl. Phys. Lett. **96**, 252108 (2010).
[25]J. P. Praseuth, M. C. Joncour, J. M. Gerard, P. Henoe, and M. Quiilec, "Growth and characterization of AIGalnAs lattice matched to InP grown by molecular-beam epitaxy," J. Appi. Phys. **63**(2), 400–403 (1988).
[26]P. Vogt, *Growth Kinetics, Thermodynamics, and Phase Formation of Group-III and IV Oxides During Molecular Beam Epitaxy* (Humboldt-Universität Berlin, 2017).
[27]A. Mauze, T. Itoh, Y. Zhang, E. Deagueros, F. Wu, and J. S. Speck, "Coherently strained (001) β-$(Al_xGa_{1-x})_2O_3$ thin films on β-Ga_2O_3: Growth and compositional analysis," J. Appl. Phys. **132**, 115302 (2022).
[28]J. M. Johnson, H.-L. Huang, M. Wang, S. Mu, J. B. Varley, A. F. M. Anhar Uddin Bhuiyan, Z. Feng, N. Kurian Kalarickal, S. Rajan, H. Zhao, C. G. Van de Walle, and J. Hwang, "Atomic scale investigation of aluminum incorporation, defects, and phase stability in β-$(Al_xGa_{1-x})_2O_3$ films," APL Mater. **9**, 051103 (2021).
[29]J. Åhman, G. Svensson, and J. Albertsson, "A reinvestigation of β-gallium oxide," Acta Crystallogr. C **52**, 1336–1338 (1996).
[30]J. E. N. Swallow, R. G. Palgrave, P. A. E. Murgatroyd, A. Regoutz, M. Lorenz, A. Hassa, M. Grundmann, H. von Wenckstern, J. B. Varley, and T. D. Veal, "Indium gallium oxide alloys: Electronic structure, optical gap, surface space charge, and chemical trends within common-cation semiconductors," ACS Appl. Mater. Interfaces **13**, 2807–2819 (2021).
[31]J. Huso, M. D. McCluskey, Y. Yu, M. Minhazul Islam, and F. Selim, "Localized UV emitters on the surface of β-Ga_2O_3," Sci. Rep. **10**, 21022 (2020).
[32]H. Peelaers and C. G. Van de Walle, "Sub-band-gap absorption in Ga_2O_3," Appl. Phys. Lett. **111**, 182104 (2017).
[33]H. Peelaers and C. G. Van de Walle, "Brillouin zone and band structure of β-Ga_2O_3," Phys. Status Solidi B **252**(4), 828–832 (2015).
[34]K. A. Mengle, G. Shi, D. Bayerl, and E. Kioupakis, "First-principles calculations of the near-edge optical properties of β-Ga_2O_3," Appl. Phys. Lett. **109**, 212104 (2016).
[35]T. Wang, W. Li, C. Ni, and A. Janotti, "Band gap and band offset of Ga_2O_3 and $(Al_xGa_{1-x})_2O_3$ alloys," Phys. Rev. Appl. **10**, 011003 (2018).
[36]T. Sato and E. Iwase, "High-accuracy contact resistance measurement method for liquid metal by considering current-density distribution in transfer length method measurement," ACS Appl. Mater. Interfaces **15**, 44404–44412 (2023).
[37]P. Mazzolini, P. Vogt, R. Schewski, C. Wouters, M. Albrecht, and O. Bierwagen, "Faceting and metal-exchange catalysis in (010) β-Ga_2O_3 thin films homoepitaxially grown by plasma-assisted molecular beam epitaxy," APL Mater. **7**, 022511 (2019).
[38]P. Mazzolini, C. Wouters, M. Albrecht, A. Falkenstein, M. Martin, P. Vogt, and O. Bierwagen, "Molecular beam epitaxy of β-$(In_xGa_{1-x})_2O_3$ on β-Ga_2O_3 (010): Compositional control, layer quality, anisotropic strain relaxation, and prospects for two-dimensional electron gas confinement," ACS Appl. Mater. Interfaces **16**(10), 12793–12804 (2024).
[39]P. Vogt and O. Bierwagen, "The competing oxide and sub-oxide formation in metal-oxide molecular beam epitaxy," Appl Phys. Lett. **106**, 081910 (2015).
[40]C. S. Chang, N. Tanen, V. Protasenko, T. J. Asel, S. Mou, H. G. Xing, D. Jena, and D. A. Muller, "γ-phase inclusions as common structural defects in alloyed β-$(Al_xGa_{1-x})_2O_3$ and doped β-Ga_2O_3 films," APL Mater. **9**, 051119 (2021).

18 November 2024 22:31:25

© Author(s) 2024